Publications

Available Online

J. Sci. Res. **17** (3), 717-725 (2025)

JOURNAL OF
SCIENTIFIC RESEARCH

www.banglajol.info/index.php/JSR

Uniaxial Pressure Induced Giant Piezoresistance Effect in Magnetoresistive Manganites

Prosenjit Sarkar*

Department of Physics, Serampore College, Serampore 712201, West Bengal, India

Received 27 August 2024, accepted in final revised form 18 May 2025

Abstract

The uniaxial pressure (*P*) dependence of electrical resistivity along the *ab*-plane and *c*-axis has been investigated in the single crystals of $(Sm_{1-y}Nd_y)_{0.52}Sr_{0.48}MnO_3$ for $y = 0$ and 0.3. At ambient pressure, the metal-insulator phase transition has been observed both for $y = 0$ and 0.3. With the application of external uniaxial pressure in the direction perpendicular to the *c*-axis of the crystal, the metal-insulator transition shifts towards lower temperature, while the transition temperature increases with pressure when it is applied parallel to the *c*-axis. This behaviour is quite different from that observed in the case of external hydrostatic pressure. The most remarkable thing about the present study is that a giant piezoresistance effect was observed in the vicinity of the metal-insulator transition for $y = 0.3$ crystal, which may be used for various technological applications.

Keywords: Electrical resistivity; Uniaxial pressure; Piezoresistance.

doi: https://dx.doi.org/10.3329/jsr.v17i3.75694 J. Sci. Res. **17** (3), 717-725 (2025)

1. Introduction

Perovskite manganites $RE_{1-x}AE_xMnO_3$ (*RE*: rare-earth ions, *AE*: alkaline-earth ions) have been the focus of intense research since the discovery of the colossal magnetoresistance effect, which has already made them a potential candidate in the field of magnetoresistance sensors [1-23]. Two important factors mainly determine the magnetoresistive properties of mixed valance manganites: the e_g-electron bandwidth and the quenched disorder [8-10]. The bandwidth of the system is controlled by the Mn-O bond length and Mn-O-Mn bond angle, whereas the size difference between RE and AE ions determines quenched disorder. Several studies have shown that narrowband manganites with large disorder exhibit exotic phase diagrams [3-8].

In prototypical $Sm_{1-x}Sr_xMnO_3$, the effects of local disorder on magnetic and electronic properties have been well studied, which reveals that the nature of electronic and magnetic phase diagrams of $Sm_{1-x}Sr_xMnO_3$ ($x = 0.48$) can be modulated by applying external

---

[*] *Corresponding author*: psphysics1981@gmail.com

perturbations like pressure and magnetic field [1-3,5,22,24]. When external hydrostatic pressure is applied, the unit cell of the system is compressed along every axis, but on the other hand, uniaxial pressure compresses the lattice only in the direction along which it is applied and simultaneously expands the unit cell in the other two directions.

The systems investigated here are $(Sm_{1-y}Nd_y)_{0.52}Sr_{0.48}Mn0_3$ (y=0 and 0.3), orthorhombically distorted narrowband perovskite manganites. The present systems are very close to the charge-ordered state, so they are extremely sensitive to external mechanical stresses. In the literature, several reports exist on the effect of hydrostatic pressure on charge ordering, metal-insulator transition, and magnetic states in manganites [1-2,5-16]. However, there are few reports on uniaxial pressure studies [1-5]. Here, we report the uniaxial pressure-dependent transport measurements on oriented single crystals for both the $P \parallel c$-axis and the $P \parallel ab$-plane. The experimental measurements were performed on single crystals rather than polycrystalline samples to avoid the effect of grain boundaries on the samples. In the present work, the uniaxial pressure dependence of resistivity for $(Sm_{1-y}Nd_y)_{0.52}Sr_{0.48}Mn0_3$ with y = 0 and 0.3 has been extensively studied. The analysis of experimental data reveals that the system behaves differently in different directions. The system with y = 0.3 exhibits a large piezoresistance (the change in electrical resistance with externally applied pressure) effect at a relatively low pressure along the c-axis of the crystal.

2. Experimental Procedure

The single crystals of $(Sm_{1-y}Nd_y)_{0.52}Sr_{0.48}Mn0_3$ with y = 0 and 0.3 were prepared by the travelling solvent floating zone (TSFZ) technique by using an image furnace as shown in Fig. 1. We have used the TSFZ image furnace with two hemielliptic focusing mirrors. The apparatus is equipped with the heat source of incandescent halogen lamps installed at one focal point of the hemielliptic mirrors, whose inside surface is totally gold-plated to enhance its reflectance. Infrared rays irradiated from the reflector are converged to a point, producing a sufficient amount of heat to melt the sample, forming a molten (floating) zone. Two shafts (upper and lower) can move up and down independently or in synchronized mode.

The polycrystalline powder, prepared by solid state reaction technique, was formed into a cylindrical shape with ~5 mm in diameter and ~10 cm length with the use of hydrostatic pressure of 5 tons and fired at 1350°C for 20 hours in air. Then, the rod was divided into two pieces and fitted into the upper and lower shaft as a feed and seed rod, respectively. The feed and seed rods were moved down and upward until they touched each other. A suitable voltage was applied to the lamps by the lamp output voltage control unit operated by a computer, so that the produced heat can melt the junction region of the rods and form a molten zone that is maintained between two rods of the solid without any container. The molten part stabilizes due to the balance between the surface tension force and the gravitational force. Then the feed and seed rods were rotated in the opposite direction at the rate of 25 rpm. A single crystal can be grown by moving the molten zone slowly downward with a growth rate of 8-10 mm/h. The growth takes place inside a quartz tube in an oxygen atmosphere.

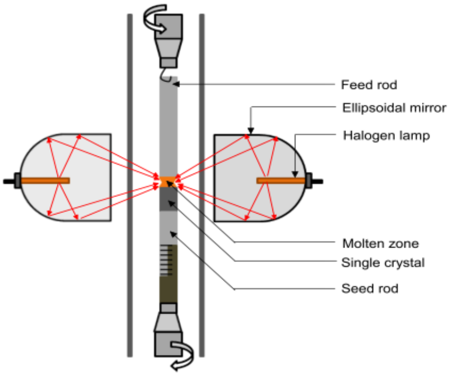

Fig. 1. Schematic diagram of the floating zone technique for the preparation of single crystalline samples.

Thus, we prepared the single crystals of $(Sm_{1-y}Nd_y)_{0.52}Sr_{0.48}Mn0_3$ with $y = 0$ and 0.3. To characterize the samples, we have used powder X-ray diffraction (XRD) and Laue diffraction techniques. Samples for powder XRD were prepared by grinding the samples and pressing them on a glass holder to achieve a smooth, flat surface. We have measured the diffraction data using the diffractometer in reflection mode. Using an automated goniometer, step-by-step scattered intensity has been measured, and the recorder gives an intensity count vs. 2θ plot. Fig. 2 shows the XRD pattern for $(Sm_{1-y}Nd_y)_{0.52}Sr_{0.48}Mn0_3$ with $y = 0$ at room temperature. The diffraction pattern can be well indexed on the basis of the orthorhombic structure with *Pbnm* space group. The lattice parameters obtained from the Rietveld refinements are $a = 5.4414$ Å, $b = 5.4176$ Å, and $c = 7.6521$ Å, which are comparable with those reported by Tomioka *et al.* [3].

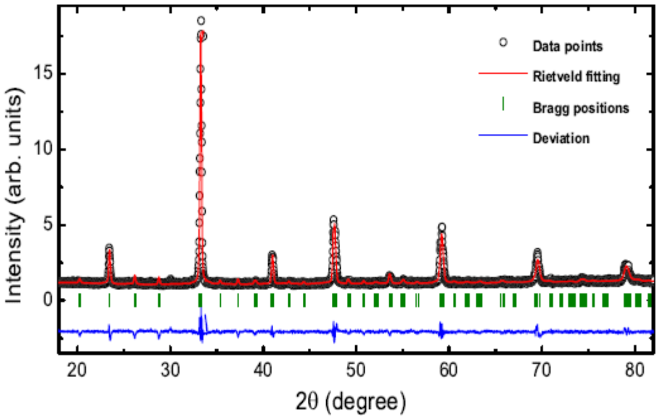

Fig. 2. XRD pattern of $Sm_{0.52}Sr_{0.48}MnO_3$ [$(Sm_{1-y}Nd_y)_{0.52}Sr_{0.48}Mn0_3$ with $y = 0$] at room temperature. The red line corresponds to the Rietveld refinement of the diffraction pattern with space group *Pbnm*.

In powder XRD, a finely powdered specimen is placed in the monochromatic beam of X-rays. Just by chance, some of its microcrystals are oriented at the correct diffraction angle θ for a particular set of (*hkl*) planes obeying Bragg's law, and corresponding diffraction peaks are observed. Bragg's law can also be satisfied by varying wavelength λ instead of θ. In the Laue method, a single crystal specimen is held stationary in a beam of x-rays of continuous wavelength. Each set of crystal planes chooses its own wavelength from the incident beam and satisfies Bragg's law. The diffraction pattern consists of a series of spots, basically a map of the crystal's reciprocal lattice under the experiment. As the symmetry properties of the reciprocal lattice are directly related to the symmetry properties of the direct lattice, the pattern must show the symmetry of the crystal in the used orientation. Thus, the Laue pattern is convenient for checking the orientation of the crystals. There are two types of the Laue method: the transmission method and the back reflection method. In transmission method, the diffracting crystal lies between the source and the recording screen, where as screen is located between the source and the crystal in case of back reflection technique, in which x-ray passes the screen through a pin-hole arrangement, reaches to crystal, diffracts, and then produces a series of spots on the screen. The crystal orientation is determined from the position of the spots by indexing them using the Greninger chart. $Sm_{0.52}Sr_{0.48}MnO_3$ crystal was oriented using the Laue back reflection method and is shown in Fig. 3.

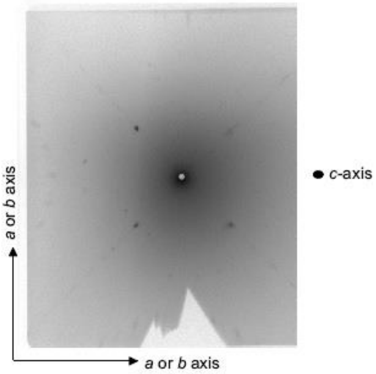

Fig. 3. Laue back reflection image of *c*-axis of $Sm_{0.52}Sr_{0.48}MnO_3$ [$(Sm_{1-y}Nd_y)_{0.52}Sr_{0.48}Mn0_3$ with y = 0] at room temperature.

Both powder X-ray diffraction and Laue diffraction data reveal high purity of the crystals. The electrical resistivity was measured by the standard four-probe technique. The uniaxial pressure was applied along the *ab*-plane and *c*-axis direction. A calibrated Cernox sensor was used to measure the sample temperature. Here, pressure was calculated directly from the surface area of the crystal, the rotations of the disk micrometer, and the force-constant value of the spring.

3. Results and Discussion

Figs. 4(a) and (b) show the temperature dependence of ρ_c and ρ_{ab} of $(Sm_{1-y}Nd_y)_{0.52}Sr_{0.48}Mn0_3$ single crystal with $y = 0$. ρ_{ab} and ρ_c have been measured by applying uniaxial pressure in the direction parallel and perpendicular to the *c*-axis of the crystal, respectively. As temperature lowers, both ρ_c and ρ_{ab} increase exponentially up to the metal-insulator transition (MIT) temperature, T_{MI}, and then drop very sharply just below T_{MI}. MIT is significantly affected by the application of uniaxial pressure in both parallel and perpendicular directions to the *c*-axis of the crystal. With the increment of uniaxial pressure for $P\perp$c, MIT moves toward the lower temperature. The effect of pressure on ρ_c is largest just a few Kelvin below the T_{MI}, where it rapidly increases with increasing *P,* but the peak resistivity of ρ_c remains almost unaltered. In contrast to ρ_c , $\rho_{ab}(T)$ shows that both T_{MI} and the value of resistivity in the insulator phase increase slowly with the increase of *P*. In Fig. 4(c), the pressure dependence of T_{MI} for y=0 has been depicted. It is clear from the Fig. 4(c) that T_{MI} increases almost in a linear fashion at the rate of ~17 K/GPa for $P\|$ c, while it decreases linearly at the rate of ~39 K/GPa for $P\perp$c. In Fig. 4(d), the ratio of peak resistivities for both $P\|$ c and $P\perp$c has been plotted. It is clear from the Fig. 4(d) that the ratio of peak values of resistivities, $\rho_m(P)/\rho_m(0)$, increases very sharply with applied external pressure for ρ_{ab}, while for ρ_c, the increment is relatively less. Here, $\rho_m(0)$ and $\rho_m(P)$ represent the peak values of resistivity at ambient and under uniaxial pressure, respectively.

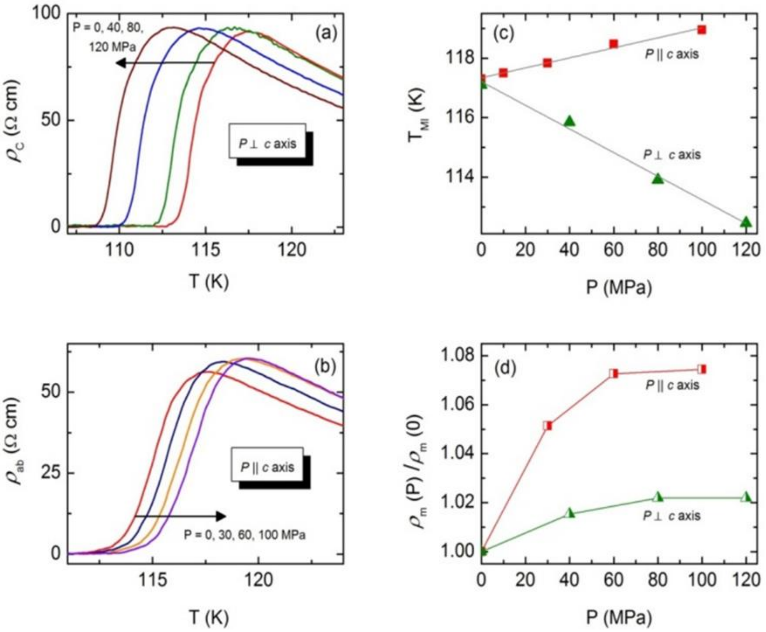

Fig. 4. Temperature dependence of (a) *c*-axis (ρ_c) and (b) *ab*-plane (ρ_{ab}) resistivities of $(Sm_{1-y}Nd_y)_{0.52}Sr_{0.48}Mn0_3$ ($y = 0$) single crystal under various uniaxial pressures. Data taken in the heating cycle are shown. (c) Uniaxial pressure dependence of metal-insulator transition temperature, T_{MI}. (d) Ratio of peak resistivities for *P* parallel and perpendicular to the *c*-axis of the crystal.

This behavior is quite distinct from that observed in hydrostatic pressure [24] and has been explained by taking into account the change in equatorial and apical Mn-O-Mn bond angles with the application of external pressure. When hydrostatic pressure is applied, the Mn-O bond length decreases, whereas the Mn-O-Mn bond angle increases. Both these effects increase the charge transfer process, and T_{MI} increases with hydrostatic pressure. For uniaxial pressure, one has to consider the anisotropy between equatorial and apical Mn-O-Mn bond angles. For orthorhombic crystal structure, as the deviation of the Mn-O-Mn bond angle from colinearity is larger along the apical direction as compared to the ab-plane, the physical properties of the system are expected to be more responsive to the change in Mn-$\mathrm{O_{ap}}$-Mn than Mn-$\mathrm{O_{eq}}$-Mn. When the external pressure is applied perpendicular to the *c*-axis, the equatorial and apical Mn-O-Mn bond angles increase and decrease, respectively, while the Mn-O bond length along the *c*-axis increases [2-5]. As the effect of change along the *c*-axis is large, we observe a large decrease of T_{MI} with pressure. We would like to mention that no straightforward explanation exists for the increase of T_{MI} with pressure when applied parallel to the c-axis. However, studying the uniaxial pressure-dependent change in the crystal structure is important to understand the correlation between structural and transport properties properly.

Fig. 5 displays the temperature dependence of ρ_c and ρ_{ab} of $(\mathrm{Sm}_{1-y}\mathrm{Nd}_y)_{0.52}\mathrm{Sr}_{0.48}\mathrm{MnO}_3$ single crystal with $y = 0.3$ for different uniaxial pressures. The pressure dependence of ρ_c and ρ_{ab} for $y = 0.3$ is almost similar to the $y = 0$ crystal, but the value of T_{MI} for ambient pressure is enhanced for $y = 0.3$. As Nd is substituted, the bandwidth of the system increases, whereas quenched disorder decreases, and as a result, T_{MI} increases with Nd doping [8,9].

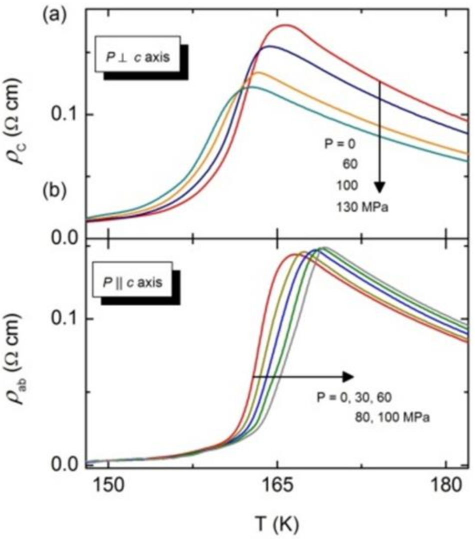

Fig. 5. Temperature dependence of *c*-axis (ρ_c) and *ab*-plane (ρ_{ab}) resistivities of $(\mathrm{Sm}_{1-y}\mathrm{Nd}_y)_{0.52}\mathrm{Sr}_{0.48}\mathrm{MnO}_3$ ($y = 0.3$) single crystal under various uniaxial pressures. Data taken in the heating cycle are shown.

Furthermore, the temperature dependence of resistivity both for $y = 0$ and 0.3 have been analyzed. For $T > T_{MI}$, both ρ_c and ρ_{ab} follow an activated-like behaviour $\rho \sim \exp(E_g/k_B T)$, where E_g is the activation energy. The value of E_g reduces from 102 meV to 87 meV as y increases from 0 to 0.3. This fact indicates that the partial substitution of Nd at the Sm site suppresses the formation of the polaronic state, increases the carrier mobility, and stabilizes the metallic phase. Therefore, both the conductivities and T_{MI} are enhanced. Several studies on perovskite and bilayer manganites have shown direct evidence of the existence of polarons by using neutron diffraction, electron paramagnetic resonance, optical conductivity spectra, etc. [16-23].

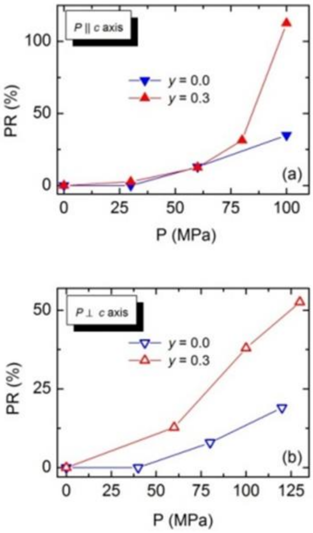

Fig. 6. Uniaxial pressure dependence of piezoresistance (PR) of $(Sm_{1-y}Nd_y)_{0.52}Sr_{0.48}Mn0_3$ with $y = 0$ and 0.3.

It is clear from Fig. 5 that the resistivity for $y = 0.3$ crystal changes dramatically with uniaxial pressure. In order to quantify these changes, the piezoresistance (PR) have been computed as $\Delta\rho/\rho(P) = [\rho(0) - \rho(P)]/\ \rho(P)$, where $\rho(0)$ and $\rho(P)$ represent the resistivity values at ambient and under uniaxial pressure, respectively. Figs. 6(a) and 6(b) depict the pressure dependence of PR for $y = 0$ and 0.3 crystals, both parallel and perpendicular to the *c*-axis of the crystal, respectively. For P∥c, PR for $y = 0$ exhibits minimal changes with increasing uniaxial pressure, whereas it rapidly increases with pressure for $y = 0.3$. For P=100 MPa, the PR value becomes more than 100 %. Such a giant piezoresistance effect can be viewed as a switching-like behavior between high-resistive and low-resistive states, which can have technological applications. On the other hand, for P⊥c, PR for y=0 system increases with P almost in the same fashion as that of for P∥c, and PR for y=0 system increases with P rapidly and reaches 50 % for P=125 MPa. In this context, it may be useful to compare the present results with the effect of hydrostatic pressure on resistivity in manganite systems [17-24]. Generally, hydrostatic pressure suppresses resistivity both in metallic and insulating phases, but its effects are much stronger in the vicinity of T_{MI}, resulting in PR exhibiting a peak close to T_{MI}, as in the case of magnetoresistance.

4. Conclusion

The temperature and uniaxial pressure dependency of *ab*-plane and *c*-axis resistivity in the single crystals of $(Sm_{1-y}Nd_y)_{0.52}Sr_{0.48}Mn0_3$ with y=0 and 0.3 have been studied. For y=0, as uniaxial pressure is applied along the *c*-axis of the crystal, the metal-insulator transition shifts toward the higher temperature almost linearly at the rate of 17 K/GPa, whereas T_{MI} decreases at the rate of 39 K/GPa, when pressure is applied perpendicular to the *c*-axis. With Nd doping, i.e., with increasing y, dT_{MI}/dP increases for $P\| c$ and decreases for $P\perp c$, respectively. This system also displays a giant piezoresistance effect near the metal-insulator transition for y=0.3 crystal at a relatively low value of applied pressure along the *c* axis, which unveils a wide range of potential applications with pressure as a control parameter.

Acknowledgment

The author would like to acknowledge P. Mandal for his help in preparing the samples and for collecting the experimental data.

References

1. T. Arima and K. Nakamura, Phys. Rev. B **60**, R15013 (1999). https://doi.org/10.1103/PhysRevB.60.R15013
2. H. Kuwahara, Y. Moritomo, Y. Tomioka, A. Asamitsu, M. Kasai, R. Kumai, and Y. Tokura, Phys. Rev. B **56**, 9386 (1997). https://doi.org/10.1103/PhysRevB.56.9386
3. Y. Tomioka, H. Hiraka, Y. Endoh, and Y. Tokura, Phys. Rev. B **74**, ID 104420 (2006). https://doi.org/10.1103/PhysRevB.74.104420
4. B. Dabrowski, X. Xiong, Z. Bukowski, R. Dybzinski, P. W. Klamut et al., Phys. Rev. B **60**, ID 7006 (1999). https://doi.org/10.1103/PhysRevB.60.7006
5. L. Demko, I. Kezsmarki, G. Mihaly, N. Takeshita, Y. Tomioka, and Y.Tokura, Phys. Rev. Lett. **101**, ID 037206 (2008). https://doi.org/10.1103/PhysRevLett.101.037206
6. S. Mandal, S. Mohanty, S. Chakravarty, and S. Mukherjee, J. Chem. Phys. **160**, 214201 (2024). https://doi.org/10.1063/5.0204312
7. P. R. Nadig, M. S. Murari, and M. D. Daivajna, Phys. Chem. Chem. Phys. **26**, 5237 (2024). https://doi.org/10.1039/d3cp04185a
8. L. M. Rodriguez-Martinez and J. P. Attfield, Phys. Rev. B **54**, ID R15622 (1996). https://doi.org/10.1103/PhysRevB.54.R15622
9. R. Das, S. Pal, S. Bhattacharya, S. Chowdhury, K. K. M. Supin et al., Phys. Rev. Mater. **7**, ID 024411 (2023). https://doi.org/10.1103/PhysRevMaterials.7.024411
10. P. G. Radaelli, G. Iannone, M. Marezio, H. Y. Hwang, S.-W. Cheong et al., Phys. Rev. B **56**, 8265 (1997). https://doi.org/10.1103/PhysRevB.56.8265
11. V. E. Salazar-Muñoz, A. L. Guerrero, and S. A. Palomares-Sánchez, J. Magn. Magn. Mater. **562**, ID 169787 (2022). https://doi.org/10.1016/j.jmmm.2022.169787
12. A. K. Saw, S. Hunagund, R. L. Hadimani, and V. Dayal, Mater. Today: Proceed. **46**, 6218 (2021). https://doi.org/10.1016/j.matpr.2020.04.766

13. F. Rivadulla, M. Otero-Leal, A. Espinosa, A. de Andres, C. Ramos et al., Phys. Rev. Lett. **96**, ID 016402 (2006). https://doi.org/10.1103/PhysRevLett.96.016402
14. H. Roder, J. Zang, and A. R. Bishop, Phys. Rev. Lett. **76**, 1356 (1996). https://doi.org/10.1103/PhysRevLett.76.1356
15. S. J. L. Billinge, R. G. DiFrancesco, G. H. Kwei, J. J. Neumeier, and J. D. Thompson, Phys. Rev. Lett. **77**, 715 (1996). https://doi.org/10.1103/PhysRevLett.77.715
16. J. M. De Teresa, M. R. Ibarra, P. A. Algarabel, C. Ritter, C. Marquina et al., Nature (London) **386**, 256 (1997). https://www.nature.com/articles/386256a0
17. A. Shengelaya, G.-m. Zhao, H. Keller, and K. A. Muller, Phys. Rev. Lett. **77**, 5296 (1996). https://doi.org/10.1103/PhysRevLett.77.5296
18. L. Vasiliu-Doloc, S. Rosenkranz, R. Osborn, S. K. Sinha, J. W. Lynn et al., Phys. Rev. Lett. **83**, 4393 (1999). https://doi.org/10.1103/PhysRevLett.83.4393
19. K. H. Kim, J. H. Jung, and T. W. Noh, Phys. Rev. Lett. **81**, 1517 (1998). https://doi.org/10.1103/PhysRevLett.81.1517
20. M. Jaime, M. B. Salamon, M. Rubinstein, R. E. Treece, J. S. Horwitz, and D. B. Chrisey, Phys. Rev. B **54**, 11914 (1996). https://doi.org/10.1103/PhysRevB.54.11914
21. M. Jaime, M. B. Salamon, K. Pettit, M. Rubinstein, R. E. Treece et al., Appl. Phys. Lett. **68**, 1576 (1996). https://doi.org/10.1063/1.116686
22. T. T. M. Palstra, A. P. Ramirez, S.-W. Cheong, B. R. Zegarski, P. Schiffer, and J. Zaanen, Phys. Rev. B **56**, 5104 (1997). https://doi.org/10.1103/PhysRevB.56.5104
23. M. Jaime, H. T. Hardner, M. B. Salamon, M. Rubinstein, P. Dorseyand, and D. Emin, Phys. Rev. Lett. **78**, 951 (1997). https://doi.org/10.1103/PhysRevLett.78.951
24. P. Sarkar, P. Mandal, A. K. Bera, S. M. Yusuf, S. Arumugam et al., Phys. Rev. B **79**, 144431 (2009). https://doi.org/10.1103/PhysRevB.79.144431